EUROPEAN ORGANIZATION FOR NUCLEAR RESEARCH

CERN/EP 86-122
FERMILAB-PUB-86/112-E
10 September 1986

INCLUSIVE CHARM CROSS SECTIONS IN 800 GeV/c p-p INTERACTIONS

LEBC-MPS Collaboration

R. Ammar[8], S. Banerjee[3], J.F. Baland[11], S. Ball[8], R.C. Ball[9], P.C. Bhat[6], C. Bromberg[10], R. Brun[12], G.E. Canough[12], T. Coffin[9], V. Commichau[1], R. Davis[8], T.O. Dershem[9], R.L. Dixon[7], H.C. Fenker[7], S.N. Ganguli[3], U. Gensch[2], N. Giokaris[12], P. Girtler[14], A.T. Goshaw[6], J. Gress[8], A. Gurtu[3], V.P. Henri[11], J.J. Hernandez[5], J. Hrubec[5], M. Iori[5], L.W. Jones[9], D. Knauss[2], D. Kuhn[14], N. Kwak[8], I.D. Leedom[9(*)], P. Legros[11], J. Lemonne[4], H. Leutz[5], X. Liu[8], P.K. Malhotra[3], J.M. Marraffino[13], G.E. Mendez[6], S. Mikocki[12], R. Miller[10], T. Naumann[2], G. Neuhofer[14], A. Nguyen[10], M. Nikolic[7(**)], H. Nowak[2], P. Pilette[11], A. Poppleton[5], J. Poirier[12], R. Raghavan[3], K. Rasner[14], S. Reucroft[5(***)], W.J. Robertson[6], B.P. Roe[9], C.E. Roos[13], A. Roth[1], M. Senko[13], W. Struczinski[1], A. Subramanian[3], M.C. Touboul[5], B. Vonck[4], L. Voyvodic[7], W.D. Walker[6], J.W. Waters[13], M.F. Weber[9], M.S. Webster[13], J. Wickens[4], C.F. Wild[6] and S. Youtsey[7]

1 III. Physikalisches Institut der Technischen Hochschule, Aachen, FRG
2 Institut für Hochenergiephysik der AdW der DDR, Berlin-Zeuthen, GDR
3 Tata Institute of Fundamental Research, Bombay, India
4 Inter-University Institute for High Energies (ULB-VUB), Brussels, Belgium
5 CERN, European Organization for Nuclear Research, Geneva, Switzerland
6 Duke University, Durham, NC 27706, USA
7 Fermilab, Batavia, IL 60510, USA
8 University of Kansas, Lawrence, KS 66045, USA
9 University of Michigan, Ann Arbor, MI 48109, USA
10 Michigan State University, East Lansing, MI 48824, USA
11 Université de l'Etat à Mons, Mons, Belgium
12 University of Notre Dame, South Bend, IN 46556, USA
13 Vanderbilt University, Nashville, TN 37235, USA
14 University of Innsbruck, Innsbruck, Austria
Oesterreich. Akad. der Wissenschaften, Vienna, Austria

Submitted to Physics Letters B

(*) Now at Fermilab, Batavia, IL. 60510, USA.
(**) On leave of absence from the Inst. of Nucl. Phys. Novi Sad, Yugoslavia.
(***) Now at Northeastern University, Boston, MA 02115, USA.

EP/2731P/SR/mk

ABSTRACT

We report a measurement of the inclusive $D/\bar{D}$ production cross section in 800 GeV/c proton-proton interactions. The experiment used the high resolution bubble chamber LEBC exposed to an 800 GeV/c proton beam at the Fermilab MPS. Comparison with 400 GeV/c pp data obtained with LEBC at CERN shows a $D/\bar{D}$ cross section increase by a factor of $1.7\ ^{+0.6}_{-0.5}$. This is in good agreement with fusion model calculations.

Charm hadroproduction cross sections have been determined in many experiments at many different energies [1]. Unfortunately most experiments operate with either low acceptance spectrometers and/or heavy material targets; most cross section determinations suffer from very large corrections. Hydrogen as target material has two noteworthy advantages. There is no atomic number correction needed to obtain the pp cross section and decays can be unambiguously distinguished from secondary interactions since the total number of charged particles leaving the secondary vertex can be reliably determined. The experiments with the smallest correction factor used the hydrogen bubble chamber LEBC and the CERN multiparticle spectrometer EHS in 360 and 400 GeV/c proton beams at CERN [2,3]. Comparison of the LEBC-EHS data at $\sqrt{s} \sim 26$–27 GeV with ISR data at $\sqrt{s} \sim 50$–60 GeV [4] indicates a cross section increase by at least a factor of 10.

In this paper we present the first charm results from Fermilab experiment E743. This experiment also used LEBC but with the Fermilab multiparticle spectrometer (MPS) in an 800 GeV/c proton beam. With $\sqrt{s} = 39$ GeV, E743 falls half way in energy between the LEBC-EHS and ISR experiments and constitutes an important check of the rising charm cross section noted above. The results presented here are based on the scanning of about 25% of the total data sample. A previous publication [5] contains results on the charged particle multiplicity distribution at this energy.

The bubble chamber LEBC was specially designed for the study of charm particle properties in the fixed target environment [2,3,5]. The two view conventional optical system of LEBC provides a resolved bubble diameter of 20 μm. Thus the two track resolution is ~ 20 μm and the single measurement precision ~ 2 μm. This high resolution yields a high efficiency for the detection of charm decay vertices.

The camera flash system and MPS readout were activated by an interaction trigger which used scintillators to define a good beam particle and two high resolution (500 μm pitch) multiwire proportional chambers to define a secondary multiplicity greater than 2. The same trigger was used in the CERN experiments. A total of 1 180 000 good triggers were recorded between May and August 1985 containing 500 000 hydrogen events.

The results presented here are based on a double scan of 275 000 LEBC photographs. The analysis does not use any information from the MPS. Detailed characteristics of the MPS, as configured for this experiment, will be described in a future publication.

Each of the independent scans is guided by an upstream measurement of the beam track producing the trigger. After locating the predicted interaction in the hydrogen fiducial volume the overall multiplicity is recorded and a careful search made for secondary vertex candidates. Secondary vertices are classified as either Cn (charged) or Vn (neutral) where n is the number of charged particles leaving the vertex. Charm candidates have n = 1, 3, 5 for charged and n = 2, 4, 6 for neutral decays. Since the C1 and V2 decay samples suffer from large strange particle background and the C5 and V6 samples from small statistics, we base the present analysis only on C3 and V4 decays. Events with a decay vertex are retained for further analysis only if the decay vertex lies inside a space cylinder 4 mm in diameter centred on the interacting beam track and with a length extending through the whole bubble chamber. Confining the data to this region reduces the strange particle background without affecting the charm sample, since a decaying particle transverse track length is $\leq ct$, where t is the particle proper lifetime and c the speed of light. In particular we estimate that, after this charm box cut, the $K \to 3\pi$ background in the C3 sample is less than 0.2 events. Any remaining contamination in the C3 sample from Σ^+ Dalitz decays is removed by requiring an opening angle greater than 2 mr for all pairs of decay tracks. A summary of the C3 and V4 charm candidates is given in table 1.

The multiplicity distribution for a sample of interaction trigger events is given in fig. 1. Also given is the multiplicity distribution for the beam trigger data reported elsewhere [5]. The interaction trigger introduces a bias against low multiplicity events. This is seen in fig. 1 where we also plot the interaction trigger efficiency versus multiplicity. This efficiency is taken into account in calculating the sensitivity of the experiment and hence the charm cross section. It is important to emphasise that the trigger bias against low multiplicity events results in a negligible charm bias; a Monte-Carlo simulation shows that the interaction trigger loses < 1% of charm events. This is mainly because a

pair of charm decays adds, on average, an extra four charged particles to the overall multiplicity count. The total sensitivity of the experiment is 15.2 ± 0.4 events/μb; the sensitivity of the subsample discussed here is 4.0 ± 0.1 events/μb. In order to calculate the charm cross section we use the following formula

$$\sigma(D) = \frac{N_{obs}(D).W_{mc}}{S \;.\; BR \;.\; \epsilon_s}$$

where $N_{obs}(D)$ is the number of observed D decays and W_{mc} is a Monte-Carlo computed weight which accounts for the decay selection criteria described below. S is the sensitivity of the data sample and BR the branching ratio for the particular D decay mode under consideration. The scanning efficiency, ϵ_s, computed from a comparison of the two independent scans is 0.90 ± 0.05.

The decay selection criteria are designed to restrict the data to a pure sample of D events for which the overall detection probability is high. The charm box and opening angle selection described earlier reduces the strange particle background to a minimum. We now describe cuts made on the decaying particle track length and on the decay track impact parameters and angles. We define the impact parameter for each decay track as L tanθ, where L is the decay length and θ the decay track angle relative to the decaying particle direction. The decay track impact parameter distributions for the V4 and C3 samples are shown in figs 2(a) and 2(b). The curves show the expected distributions for pure D^o and $D^{\pm}$ samples with lifetimes and production characteristics as given below. It is important to notice that even before the following decay cuts the non-D contamination is small. For the cross section computations, a decay was included into N_{obs} if its decay length was ≥ 2 mm, its minimum impact parameter ≥ 20 μm, its maximum impact parameter ≥ 50 μm (100 μm) and ≤ 1 mm (2 mm) for V4 (C3). These cuts are intended to remove topologically ambiguous decays and to minimise Λ_c and D_s (formerly the F) contamination in the $D^{\pm}$ sample. In addition, to ensure good spectrometer acceptance for future momentum analysis, decays were excluded from N_{obs} if more than one of the decay tracks had either space angle ≥ 150 mr. The effects on the C3 and V4 statistics of these cuts are presented in table 1. The C3 and V4 samples, after all cuts, are pure D samples containing, at most, a few per cent of contamination.

As noted already, a Monte-Carlo technique was used to compute W_{mc}. Identical impact parameter, length and angle cuts were used in computing W_{mc} and N_{obs}. Phase space D decays were generated with the following assumed x_F and p_T behaviour:

$$\frac{d^2N}{dx_F dp_T^2} \sim (1 - x_F)^n e^{-ap_T^2}; \quad n = 5 \text{ and } a = 1.0 \text{ (GeV/c)}^{-2}$$

As was pointed out in [6], the inclusive p_T dependence of charm production appears to be independent of beam, target or energy. The mean value of p_T is always ~ 1 GeV/c; this corresponds to $a = 1.0 \text{ (GeV/c)}^{-2}$. In general, the x_F dependence goes like $(1-x_F)^n$ with different experiments finding n anywhere between 1 and 7 [6]. The value of n we choose here is that measured for charm production in 400 GeV/c pp interactions [3]. Mean D^o and $D^{\pm}$ lifetimes were assumed to be .43ps and .92ps, respectively [7]. The sensitivity of the cross section determinations to all these assumed values is discussed below. Averaged over all x_F the mean value of W_{mc} is 4.0 for the D^o sample and 2.5 for the $D^{\pm}$ sample.

The assumed branching ratios were extracted [2] from SPEAR results [8]:

$$BR(C3) = 0.43 \pm 0.10$$

$$BR(V4) = 0.17 \pm 0.04.$$

The resulting D^o and $D^{\pm}$ inclusive cross sections (for all x_F), based on the data of table 1, are:

$$\sigma(D^o/\bar{D}^o) = 26 \, ^{+21}_{-13} \, \mu b$$

$$\sigma(D^{\pm}) = 33 \pm 7 \, \mu b$$

Giving a total inclusive $D/\bar{D}$ cross section of

$$\sigma(D/\bar{D}) = 59 \, ^{+22}_{-15} \, \mu b.$$

All the quoted cross section errors are statistical in nature.

We have investigated the sensitivity of these cross section determinations to our assumed lifetimes, branching ratios and production characteristics (x_F and p_T behaviour). The D^o and $D^{\pm}$ lifetimes

are known with an uncertainty of ~ 10% [7]. Varying the lifetimes in the Monte-Carlo within ± 10% changes the D cross section results by ~ ± 5%; a negligible systematic uncertainty. The branching ratio uncertainties are more serious. A 25% branching ratio uncertainty causes a systematic 25% cross section uncertainty. The values used here [2] have been confirmed independently [9]. However, more precise values are needed before accurate absolute cross sections can be quoted. The cross section values are very insensitive to the assumed p_T and x_F behaviour. Variations of ~ 50% in the parameters a and n cause changes in cross section of less than 10%.

Using an identical technique the NA27 collaboration [3] obtains the following cross sections (for all x_F) in 400 GeV/c pp interactions(*) ($\sqrt{s}$ = 27.4 GeV):

$$\sigma(D^0/\bar{D}^0) = 21.9 \pm 4.0 \ \mu b$$

$$\sigma(D^{\pm}) = 12.5 \pm 1.4 \ \mu b.$$

Giving a total inclusive $D/\bar{D}$ cross section for all x_F of:

$$\sigma(D/\bar{D}) = 34.4 \pm 4.2 \ \mu b.$$

Again, all the cross section errors are statistical.

These cross section values give the following ratios of cross sections

$$\frac{\sigma(D^{\pm} \text{ at } \sqrt{s} = 38.8 \text{ GeV})}{\sigma(D^{\pm} \text{ at } \sqrt{s} = 27.4 \text{ GeV})} = 2.6 \pm 0.6$$

$$\frac{\sigma(D^0/\bar{D}^0 \text{ at } \sqrt{s} = 38.8 \text{ GeV})}{\sigma(D^0/\bar{D}^0 \text{ at } \sqrt{s} = 27.4 \text{ GeV})} = 1.2 \ ^{+1.0}_{-0.6}$$

If we make the assumption that the increase in cross section with $\sqrt{s}$ is the same for neutral and charged D, we can use both ratios as independent measurements to compute the following weighted average:

$$\frac{\sigma(D/\bar{D} \text{ at } \sqrt{s} = 38.8 \text{ GeV})}{\sigma(D/\bar{D} \text{ at } \sqrt{s} = 27.4 \text{ GeV})} = 2.1 \ ^{+0.5}_{-0.4}$$

(*) The NA16 collaboration [2], using a prototype LEBC-EHS obtained $\sigma(D^0/\bar{D}^0) = 20.4 \ ^{+15.8}_{-8.6}$ μb and $\sigma(D^{\pm}) = 10.6 \ ^{+4.8}_{-3.2}$ μb at $\sqrt{s}$ = 26.0 GeV.

On the other hand, if we simply add both cross sections to obtain this ratio, we get:

$$\frac{\sigma(D/\bar{D} \text{ at } \sqrt{s} = 38.8 \text{ GeV})}{\sigma(D/\bar{D} \text{ at } \sqrt{s} = 27.4 \text{ GeV})} = 1.7 \, ^{+0.6}_{-0.5}$$

These two ratio determinations are in good agreement. The latter value does not need to assume identical energy behaviour of the $D^{\pm}$ and D^{o} cross sections and fig. 3 shows the value of this cross section ratio along with the results of fusion model calculations [10]. We choose to plot the ratio of cross sections rather than the absolute cross section values since in this way systematic branching ratio uncertainties are unimportant. As noted above, our cross section determinations are insensitive to the assumptions incorporated into the Monte-Carlo weight calculation. The cross section ratio is even less sensitive since the effects of these assumptions tend to cancel out.

The fusion model results also benefit from this method of presenting cross section versus $\sqrt{s}$. The fusion model cross section estimates depend sensitively on assumed values of different parameters (charm quark mass m_c, effective threshold $\hat{s}_{th}$ and scale parameter Λ). However, the $\sqrt{s}$ dependence of the cross section ratio is less sensitive to the values of these parameters.

The hatched band on fig. 3 shows the fusion model results. The range of values at each energy comes from using a variety of structure functions [11] and varying the charm quark mass between plausible limits (1.2 to 1.4 GeV/c^2).

At the present level of statistics, the ratio of the cross sections at $\sqrt{s}$ = 27.4 GeV and $\sqrt{s}$ = 38.8 GeV is in very good agreement with the result of a fusion model calculation. The cross section values obtained at the ISR ($\sqrt{s}$ = 52.5 GeV and $\sqrt{s}$ = 63 GeV) are typically a factor $\sim$ 10 higher than those at $\sqrt{s}$ = 27.4 GeV [4]. As can be seen from fig. 3, the fusion model calculations do not support such a rapid increase in cross section.

Acknowlegements

We would like to acknowledge the enormous support given to this experiment by Fermilab and CERN. In particular we would like to thank the CERN-LEBC group and Fermilab-EAD for their outstanding efforts on our behalf. We appreciate the important contribution made by our scanning teams and wish to thank Mu King for typing the paper.

We gratefully acknowledge the financial support of the USA teams by the DOE and NSF, of the Belgian groups by the IIKW-IISN and of the Austrian groups by FWF.

REFERENCES

[1] See, for example, A. Kernan and G. Van Dalen, Phys. Reports 106 (1984) 297.

[2] M. Aguilar-Benitez et al., Phys. Lett. 135B (1984) 237.

[3] LEBC-EHS Collaboration, Berkeley Conference preprint. Presented by M.E. Michalon and M. Iori (1986).

[4] W. Geist, Moriond Workshop on New Flavours, (Les Arcs, 1982);
L. Cifarelli, Moriond Workshop on New Flavours (Les Arcs, 1982);
W. Geist, CERN/EP 79-78 (1977);
A. Putzer, Thesis, University of Heidelberg (1984).

[5] R. Ammar et al., LEBC-MPS Collaboration, Multiplicity of charged particles in 800 GeV p-p interactions, to be published in Phys. Lett. B (1986).

[6] S. Reucroft, Proc. Int. Symp. Multiparticle Dynamics (Lake Tahoe, 1983) and CERN/EP 83-155 (1983).

[7] M. Aguilar-Benitez et al., Particle Data Group, Review of Particle Properties, Phys. Lett. 170B (1986) 1.

[8] I. Perruzzi et al., Phys. Rev. Lett. 39 (1977) 1301;
R.H. Schindler et al., Phys. Rev. D24 (1981) 78;
G.H. Trilling, Phys. Reports 75 (1981) 57.

[9] M. Aguilar-Benitez et al., Phys. Lett. 168B (1986) 170.

[10] J.R. Cudell, F. Halzen and K. Hikasa, to be published in Phys. Lett. (1986);
F. Halzen, private communication (1986).

[11] D.W. Duke and J.F. Owens, Phys. Rev. D30 (1984) 49;
M. Gluck et al., Zeitsch. für Phys. C13 (1982) 119;
E. Eichten et al., Rev. Mod. Phys. 56 (1984) 579.

TABLE CAPTION

Table 1 Summary of the charm decay sample used in the cross section determinations and the effects upon them of the selection criteria (cuts) described in the text. The numbers given are of those decays removed by the corresponding cut. The cuts are defined in the following way.

(a) Length cut: decaying particle track length greater than 2 mm.

(b) Angle cut: no more than one decay track with either space angle greater than 150 mr.

(c) Maximum impact parameter cut: maximum decay track impact parameter greater than 50 μm (100 μm) and less than 1 mm (2 mm) for V4 (C3).

(d) Minimum impact parameter cut: minimum decay track impact parameter greater than 20 μm.

TABLE 1

Topology	C3	V4
Total number of decays	34	14
Length cut	6	3
Angle cut	4	1
Maximum impact parameter cut	1	2
Minimum impact parameter cut	2	4
Total after cuts	21	4

FIGURE CAPTIONS

Fig. 1 Charged particle multiplicity distribution for a subsample of the interaction trigger data described in this paper (closed circles) and for the beam trigger data described in [5] (open circles). The distributions are normalised for $n_{ch} \geq 10$. The crosses show the interaction trigger efficiency computed by dividing the interaction trigger data by the beam trigger data. A few typical error bars are shown.

Fig. 2 Impact parameter distribution for:

(a) the V4 sample (14 decays);

(b) the C3 sample (34 decays).

The curves show the expected impact parameter distributions for pure D^{o} and $D^{\pm}$ samples. See text for details.

Fig. 3 Total $D/\bar{D}$ cross section normalised to the value at $\sqrt{s}$ = 27.4 GeV versus c.m. energy. The hatched band shows the results of fusion model calculations. As discussed in the text, the width of the band expresses the uncertainty in the fusion model parameters.

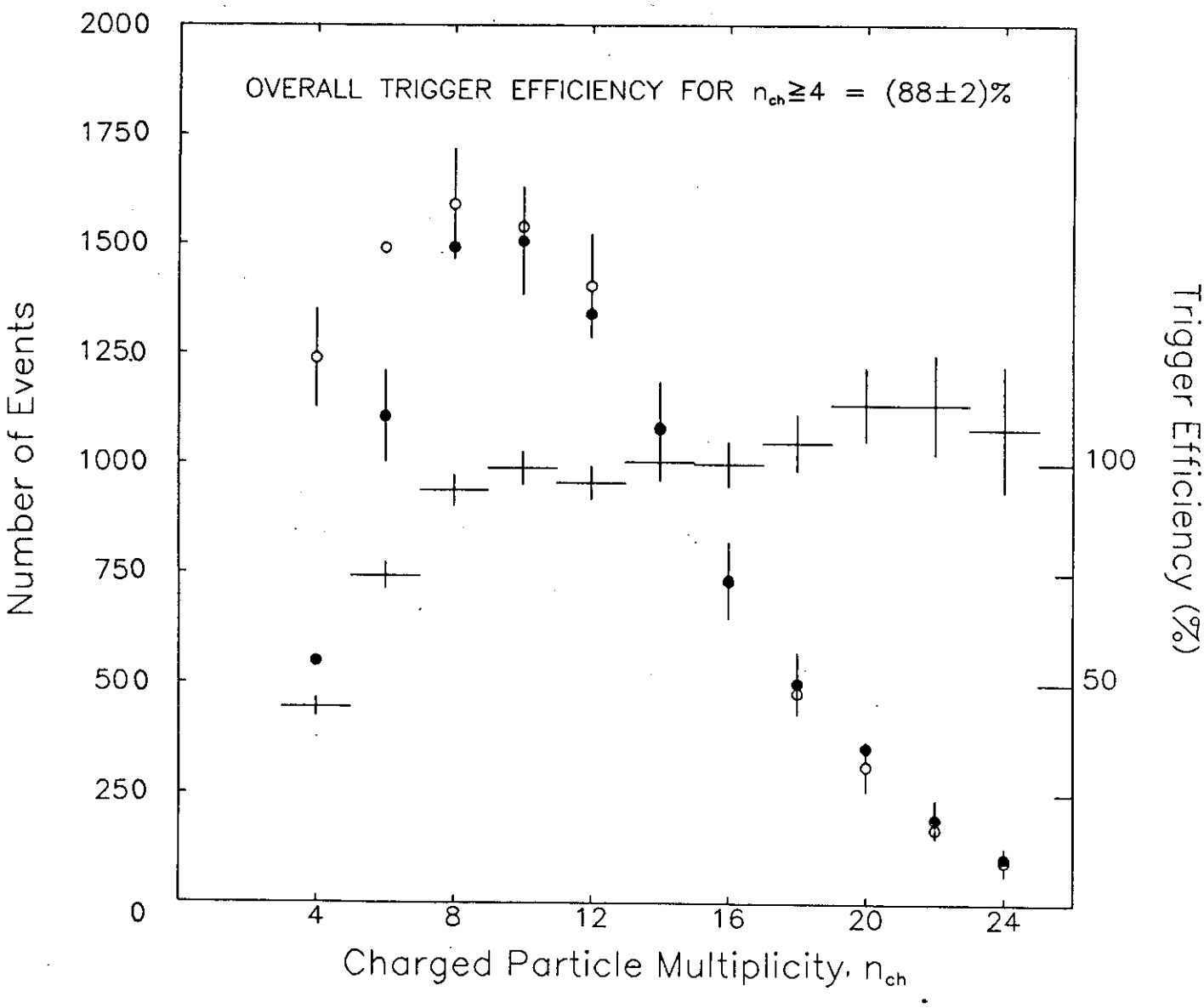
OVERALL TRIGGER EFFICIENCY FOR $n_{ch} \geq 4$ = (88±2)%
Number of Events
Trigger Efficiency (%)
Charged Particle Multiplicity, n_{ch}
2000
1750
1500
1250
1000
750
500
250
0
100
50
4
8
12
16
20
24

Fig. 1

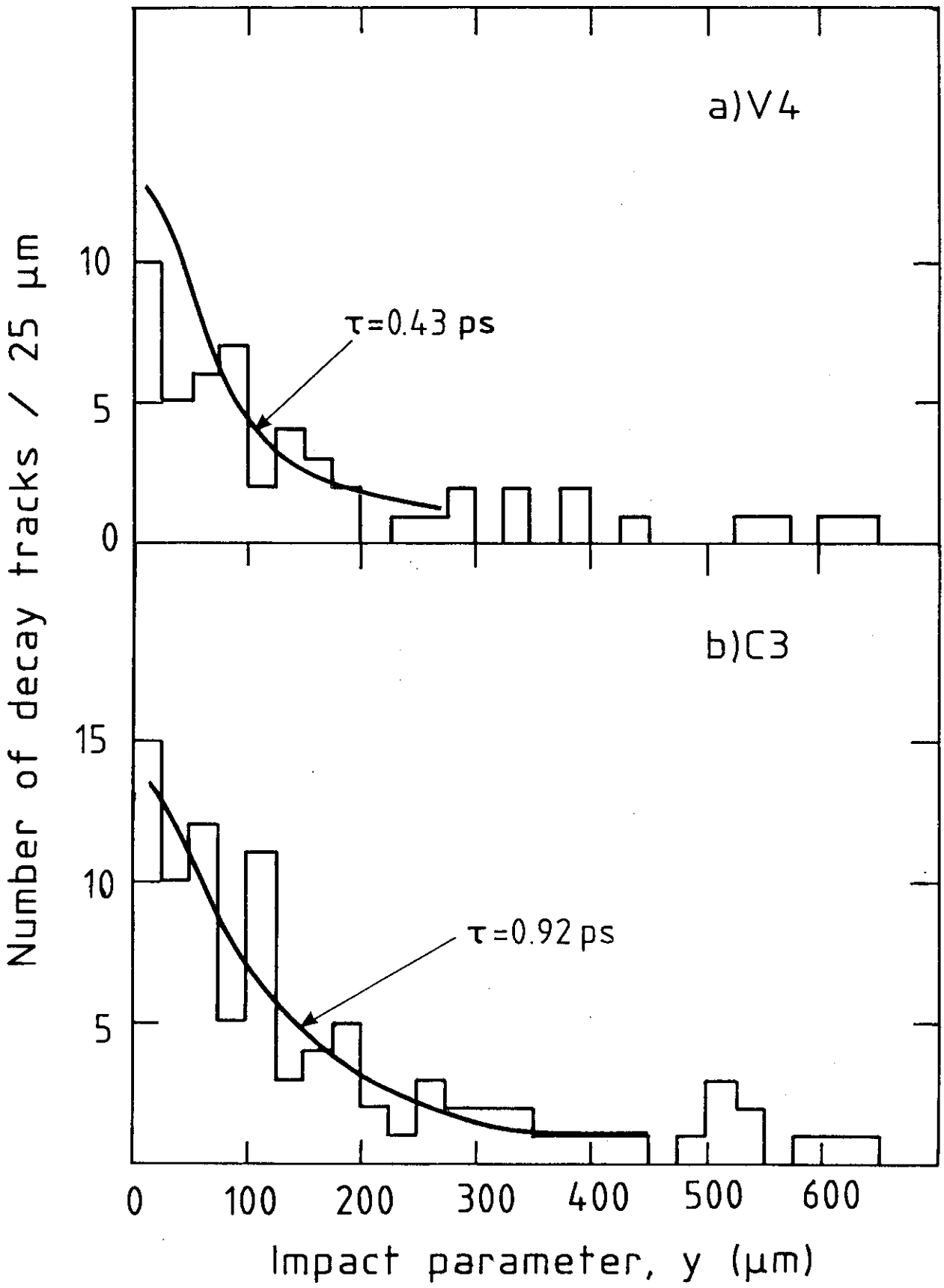
a) V4
τ=0.43 ps
b) C3
τ=0.92 ps
Number of decay tracks / 25 μm
Impact parameter, y (μm)
0
5
10
15
0
100
200
300
400
500
600

Fig. 2

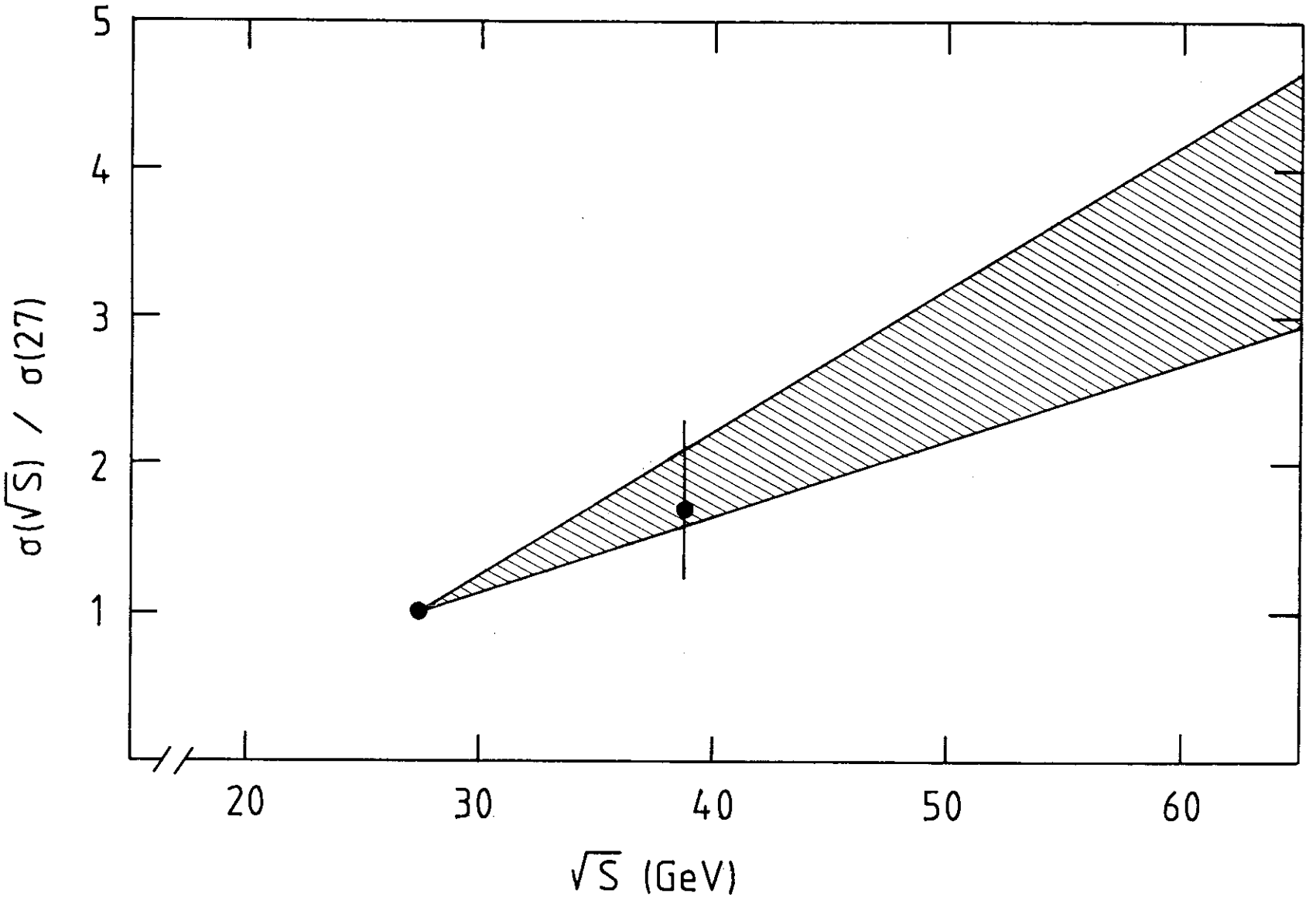

Fig. 3